Low-Field-Triggered Large Magnetostriction in Iron-Palladium Strain Glass Alloys

Shuai Ren,[1] Dezhen Xue,[1] Yuanchao Ji,[1] Xiaolian Liu,[2] Sen Yang,[1,*] and Xiaobing Ren[1,2,†]
[1]Frontier Institute of Science and Technology, and MOE Key Laboratory for Nonequilibrium Synthesis and Modulation of Condensed Matter, and State Key Laboratory for Mechanical Behavior of Materials, Xi'an Jiaotong University, Xi'an 710049, China
[2]Ferroic Physics Group, National Institute for Materials Science, Tsukuba, 305-0047 Ibaraki, Japan
(Received 23 May 2017; revised manuscript received 26 July 2017; published 22 September 2017)

Development of miniaturized magnetostriction-associated devices requires low-field-triggered large magnetostriction. In this study, we acquired a large magnetostriction (800 ppm) triggered by a low saturation field (0.8 kOe) in iron-palladium (Fe-Pd) alloys. Magnetostriction enhancement jumping from 340 to 800 ppm was obtained with a slight increase in Pd concentration from 31.3 to 32.3 at. %. Further analysis showed that such a slight increase led to suppression of the long-range ordered martensitic phase and resulted in a frozen short-range ordered strain glass state. This strain glass state possessed a two-phase nanostructure with nanosized frozen strain domains embedded in the austenite matrix, which was responsible for the unique magnetostriction behavior. Our study provides a way to design novel magnetostrictive materials with low-field-triggered large magnetostriction.

DOI: 10.1103/PhysRevLett.119.125701

Magnetostrictive materials are used as converters of electromagnetic energy into mechanical energy or vice versa. They are used extensively in traditional energy converters (sonar detector and ultrasonic imaging) as well in fashionable electronic devices (wearable devices and microelectromechanical sensors) [1–4]. To obtain smarter and more miniaturized magnetostriction-associated devices, magnetostrictive materials are currently required to have an ability to demonstrate large magnetostriction at low magnetic field [5–9].

During the past decades, many magnetostrictive materials have been developed, and the two most prominent systems include rare-earth-iron Laves phase alloys ($R_xR'_{1-x}Fe_2$, e.g., Terfenol-D) [10,11] and ferromagnetic shape memory alloys (FSMAs, e.g., Ni-Mn-Ga) [12,13]. Figure 1(a) demonstrates that $R_xR'_{1-x}Fe_2$ alloys can generate large magnetostriction of 1000–2000 ppm due to magnetic domain rotations, and have served as magnetostrictive workhorses for decades. However, their large magnetocrystalline anisotropy leads to high saturation field ($H_s > 1$ kOe), thus restricting their further applications. In contrast, FSMAs produce a giant field-induced strain (~10%) [12] due to the magnetic field induced reorientation of mesoscopic martensitic domains, and have received continuous attention since the 1990s. However, the required H_s corresponds to 10 kOe order, and is significantly larger than that of $R_xR'_{1-x}Fe_2$ alloys. Thus, these two types of magnetostrictive materials are "strong but hard" ("hard" here indicates relatively high H_s and not hard magnetic materials); i.e., their large magnetostriction is usually triggered by a high external field. Fe-Ga alloys have recently attracted significant interest since they are quite "soft" [5–8]. Field magnitude of several hundred Oersted is enough to generate relatively large magnetostriction compared to that in pure Fe. However, they are "soft but weak," for the magnetostriction is limited below 400 ppm even for a single crystal [8]. Consequently, there is a virgin region in Fig. 1(a), because magnetostrictive materials with a "soft and strong" behavior, i.e., low-field-triggered large magnetostriction, are still rare.

Herein, we report such a soft and strong behavior in Fe-Pd FSMAs. We acquired a magnetostriction as large as 800 ppm at an H_s as low as 0.8 kOe below a strain glass transition temperature (T_g) in an $Fe_{67.7}Pd_{32.3}$ directionally solidified (DS) alloy, exhibited in the virgin region [Fig. 1(a)]. This behavior is strongly related to the unique nanostructure of this strain glass alloy. Thus, this study may help to develop novel magnetostrictive materials.

$Fe_{100-x}Pd_x$ alloys with Pd concentration of $x = 30.5$–33, were prepared from high purity metals (> 99.95 at. %) by arc melting under an argon atmosphere. After solution treatment at 1273 K, the specimens underwent cold rolling, spark cutting, further solution treatment, and, finally, quenching in water. Transition latent heat was measured by a differential scanning calorimeter (DSC-Q200, TA Company). Physical property measurement system (PPMS, Quantum Design) was employed to detect magnetization. *In situ* x-ray diffraction (XRD, Shimadzu 7000 XRD) from high to low temperature was used to identify the possible structural change. Possible strain glass transition was detected by dynamic mechanical analysis (DMA-Q800, TA Instruments). The microstructure of the strain glass state was observed by transmission electron microscope (TEM, JEOL JEM-2100). DS samples were prepared by the Bridgeman method to detect the magnetostrictive behavior. The composition was determined by x-ray fluorescence (Shimadzu XRF-8000). Magnetostriction was measured by strain gauges.

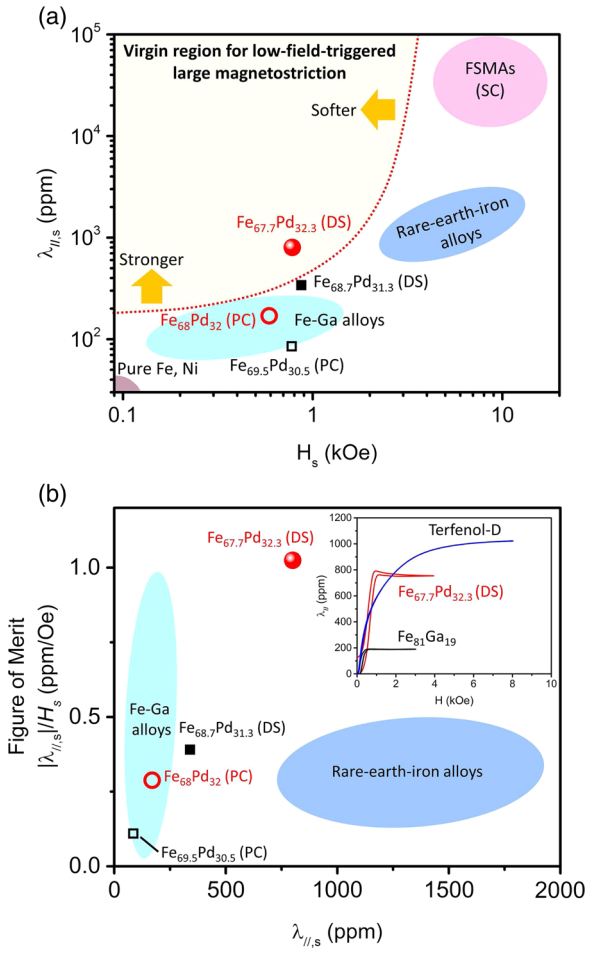

FIG. 1. (a) Comparison of the magnetostrictive benchmark ($\lambda_{||,s}$ vs H_s) between Fe-Pd alloys and main magnetostrictive families, including single crystal (SC) of FSMAs, $R_xR'_{1-x}Fe_2$ alloys, and Fe-Ga alloys. "DS" repesents Directionally solidified alloys, and "PC" strands for polycrystalline alloys. (b). Comparison of FOM among Fe-Pd alloys, $R_xR'_{1-x}Fe_2$ alloys, and Fe-Ga alloys. Inset of (b) compares the magnetostriction curves of $Fe_{67.7}Pd_{32.3}$, Terfenol-D, and $Fe_{81}Ga_{19}$ alloys.

Figure 1(a) shows H_s and saturation parallel magnetostriction ($\lambda_{||,s}$) of the current main families of magnetostrictive materials. The magnetostrictive behavior of the $Fe_{67.7}Pd_{32.3}$ DS alloy (magnetostriction of 800 ppm triggered by H_s of 0.8 kOe at 120 K) enables itself to locate in the virgin region. In contrast, the $Fe_{68.7}Pd_{31.3}$ DS alloy, with almost similar composition (only 1 at. % Pd deviation) exhibits maximum saturation magnetostriction of only 340 ppm at a similar H_s at 200 K. Clearly, a slight increase in Pd concentration resulted in significant enhancement in magnetostriction. A similar case has also been detected in polycrystalline alloys. Magnetostriction of two polycrystalline alloys, $x = 30.5$ and $x = 32$, is also shown in Fig. 1(a). Saturation magnetostriction for $x = 32$ exhibits a magnetostriction as large as 170 ppm triggered by H_s of 0.6 kOe at 180 K. Nonetheless, saturation magnetostriction for $x = 30.5$ is only 90 ppm at H_s of 0.8 kOe at 250 K [14].

To manifest the capability of magnetostrictive materials generating large magnetostriction by low H_s, we define the "figure of merit" (FOM) by $\lambda_{||,s}/H_s$. Figure 1(b) shows Fe-Ga alloys exhibit a large FOM, but the magnetostriction is small. $R_xR'_{1-x}Fe_2$ alloys generate large magnetostriction; nonetheless, the FOM is small. Notably, $Fe_{67.7}Pd_{32.3}$ DS alloy exhibits large magnetostriction together with large FOM, revealing a better combined property than that of Fe-Ga and $R_xR'_{1-x}Fe_2$ alloys. Moreover, both magnetostriction and FOM of $Fe_{67.7}Pd_{32.3}$ DS alloy are much better than those of $Fe_{68.7}Pd_{31.3}$. A similar tendency happens in polycrystalline alloys as well. The polycrystalline alloy for $x = 32$ possesses higher magnetostriction maximum together with better FOM than those for $x = 30.5$.

The inset of Fig. 1(b) compares the magnetostriction curve for $x = 32.3$ at 120 K with those of Terfenol-D and $Fe_{81}Ga_{19}$ alloys at room temperature. The $Fe_{81}Ga_{19}$ alloy undergoes easy saturation, exhibiting magnetostriction of 190 ppm at H_s of 0.5 kOe. The Terfenol-D undergoes difficult saturation, displaying magnetostriction as large as 1000 ppm at high H_s over 3 kOe. These results are consistent with data in previous studies [6,15,16]. Notably, H_s for $x = 32.3$ at 120 K is comparable with that of the $Fe_{81}Ga_{19}$ alloy; however, magnetostriction is much larger. Furthermore, magnetostriction for $x = 32.3$ is comparable with that of Terfenol-D, whereas its H_s is much smaller. Comparison of these magnetostriction curves reveals that the $Fe_{67.7}Pd_{32.3}$ DS alloy is a soft and strong magnetostrictive material.

Figure 2 shows comparison of the magnetic properties of alloys with two compositions ($x = 31.3$ and $x = 32.3$), providing details on the property jump by a slight increase in Pd concentration. Figure 2(a) shows the temperature dependence of magnetization of these two compositions. A sharp decrease is observed around 212 K for $x = 31.3$, indicating the occurrence of a first order martensitic transformation. Thus, the martensitic transformation start temperature (T_M) was determined. In contrast, the decrease in the magnetization curve of $x = 32.3$ around 130 K is much weaker than that of $x = 31.3$, indicating strong suppression of the martensitic transformation due to 1 at. % Pd deviation. Actually, there is a strain glass transition when $x \geq 32$. Thus, the temperature where weak decrease in magnetization occurs for $x = 32.3$ corresponds to T_g.

Figure 2(b) compares the temperature dependence of magnetostriction of these two compositions. Black solid squares in Fig. 2(b) represent the saturation magnetostriction (λ_s^{1st}) during the first cycle of applying and removing the magnetic field at each temperature for $x = 31.3$. It increases below T_M, while it decreases above T_M with heating. Thus, a peak at ~340 ppm appears around T_M. Noteworthy is that magnetostriction cannot completely recover after the first cycle, but becomes fully recoverable in the following cycles [Figs. 2(d2) and 2(d3)]. This part of recoverable magnetostriction (λ_s^{re}) for $x = 31.3$ is shown by black hollow squares in Fig. 2(b). λ_s^{re} exhibits a peak at ~280 ppm around T_M. Notably, deviation between the λ_s^{1st} and λ_s^{re} appears below T_M. Above T_M, they overlap with

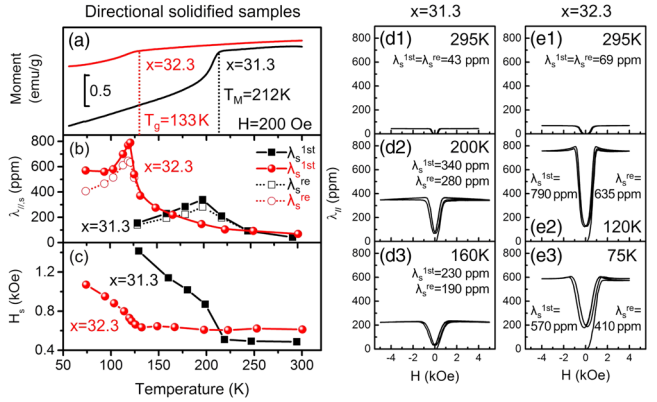

FIG. 2. (a) Temperature evolution of magnetization for $x = 31.3$ and $x = 32.3$. (b) Temperature dependence of saturation magnetostriction (λ_s^{1st}) during the first cycle and recoverable magnetostriction (λ_s^{re}) for $x = 31.3$ and $x = 32.3$. (c) Temperature dependence of H_s for $x = 31.3$ and $x = 32.3$. (d) Magnetostriction curves for $x = 31.3$ at several temperatures, 295 (d1), 200 (d2), and 160 K (d3). (e) Magnetostriction curves for $x = 32.3$ at several temperatures, 295 (e1), 120 (e2), and 75 K (e3).

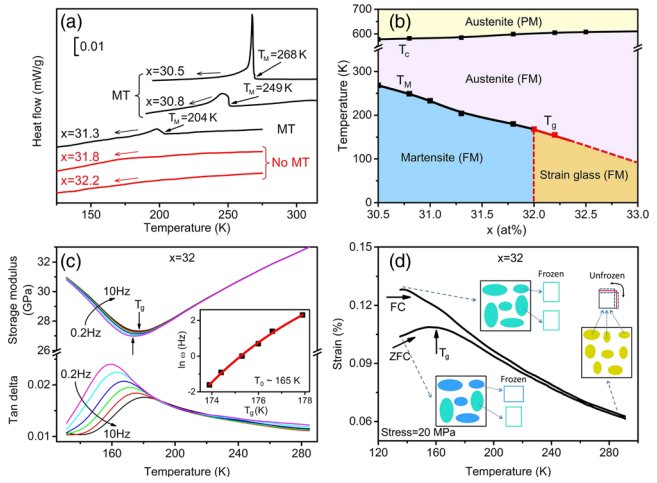

FIG. 3. (a) Evolution of heat flow curves during cooling with x variation. (b) Phase diagram of $Fe_{100-x}Pd_x$ alloys including frozen strain glass region at $x \geq 32$. (c) Frequency dispersion of storage modulus and internal friction curves during cooling for $x = 32$. The ideal freezing temperature (T_0) is yielded around 165 K by the Vogel-Fulcher relation (inset). (d) ZFC/FC curves for $x = 32$ show the broken ergodicity of strain glass. The inset figures schematically depict different frozen strain states evolved from the same unfrozen one according to their different histories, respectively.

each other because magnetostriction becomes completely recoverable, as illustrated by the magnetostriction curve at 295 K in Fig. 2(d1). According to literature [12,17], the giant field-induced strain due to reorientation of mesoscopic martensitic domains is generally unrecoverable in FSMAs. Thus, the partially recoverable magnetostriction for $x = 31.3$ indicates that the reorientation of mesoscopic martensitic domains contributes to the magnetostriction.

Interestingly, a slight modification of Pd concentration causes an impressive enhancement in λ_s. Red solid spheres represent the λ_s^{1st} during the first cycle for $x = 32.3$. Similar to the temperature tendency for $x = 31.3$, the magnetostriction also increases below T_g and decreases above T_g upon heating. Consequently, the λ_s^{1st} peak for $x = 32.3$ is ~800 ppm at 120 K, which is 150% higher than the peak for $x = 31.3$. Moreover, the magnetostriction of strain glass also partially recovers below T_g [Figs. 2(e2) and 2(e3)], and completely recovers above T_g [Fig. 2(e1)]. The λ_s^{re} exhibits a peak value around 640 ppm at 120 K, as shown by red hollow circles in Fig. 2(b). This λ_s^{re} peak for $x = 32.3$ is also much higher than the λ_s^{re} peak for $x = 31.3$.

Note that a large enhancement in magnetostriction by slight modification of Pd concentration does not lead to the increase of H_s. Figure 2(c) exhibits similar change tendency of H_s for two compositions. They both remain almost constant above the transition temperatures (T_M for $x = 31.3$ and T_g for $x = 32.3$), and increase below the transition temperatures with cooling. The field increment for $x = 32.3$ is less than that for $x = 31.3$ below the transition temperatures. In particular, the H_s for $x = 32.3$ is always less than 1 kOe above 90 K.

For obtaining the underlying reason for magnetostriction enhancement with slight composition deviation, the phase diagram of $Fe_{100-x}Pd_x$ and the supporting data are shown in Fig. 3. Figure 3(a) shows heat flow curves of different Pd concentrations with cooling. A sharp heat flow peak appears in the curve of $x = 30.5$, indicating the occurrence of a first order martensitic transformation. With the further increase in x, the heat flow peaks appear at lower temperature and become weaker and broader. It reveals that Pd atoms strongly reduce the thermodynamic stability of the martensitic phase. When x is over 31.8, the heat flow peaks become undetectable, indicating that the system enters a nontransforming region, where a strain glass transition is likely to be detected [18–20].

Figure 3(b) shows a new phase diagram of $Fe_{100-x}Pd_x$ FSMAs including a strain glass state [21,22]. The Curie temperature is around 600 K for $Fe_{69.5}Pd_{30.5}$ alloy, and slightly increases with increase in x [23]. The austenite has a face-centered cubic (fcc) phase and the martensite has a face-centered tetragonal (fct) phase [21,24]. Increasing x lowers T_M drastically, and the martensitic phase transformation disappears when $x \geq 32$ [20–24]. The high sensitivity of transition temperature on the composition may be attributed to the fact that tetragonal distortion in the Fe-Pd magnetic shape memory alloys stems from a Jahn-Teller-like effect [25]. In the nontransforming region ($x \geq 32$), glassy behavior is detected [Figs. 3(c) and 3(d)].

Figure 3(c) demonstrates that both storage modulus and tan δ at $x = 32$ exhibit frequency dependence; i.e., the dip (peak) temperatures in modulus (tan δ) curves decrease with lowering frequency. This is one typical feature of strain glass [18,19]. The Vogel-Fulcher relation ($\omega = \omega_0 \exp[-E_a/k_B(T_g - T_0)]$) captures the slowing down of dynamics during the glass transition, where ω is the oscillating frequency, ω_0 the frequency at infinitely high temperature, E_a the activation energy, T the temperature,

and T_0 the ideal freezing temperature. Here it yields T_0 around 165 K. (For details on the Vogel-Fulcher relation, please refer to Ref. [18] and references therein.) The time scale for relaxation of the nanodomains below T_0 can reach 10^2 s, obtained by fitting the so-called Cole-Cole plot [26]. (Supplemental Material, Fig. 1 [27]) Moreover, a nonsplit single peak of $(220)_{fcc}$ in XRD profiles keeps with cooling across the strain glass transition (Supplemental Material, Fig. 2 [27]), suggesting no change in average structure accompanying the strain glass transition [18,19].

Figure 3(d) shows the evidence of broken ergodicity in strain glass at $x = 32$, as indicated by zero-field-cooling (ZFC)/field-cooling (FC) measurement [28]. Ferroic glass transitions originate from the slowing down of kinetics; therefore, a glassy system freezes into a certain thermodynamic metastable state and loses the ergodicity below T_g. Breaking of ergodicity thus can be distinguished by the deviation in the FC/ZFC curves below T_g [Fig. 3(d)]. With the increase in temperature above T_g, deviation in the ZFC/FC curves gradually narrows and finally disappears, thus indicating gradual recovery of the ergodicity of the system above T_g. Similar behaviors can also be found in ferroelectric relaxor [29] and cluster spin glasses [30]. Thus, it confirms a strain glass transition for $x \geq 32$.

Strain glass has been widely discovered in SMAs [18,19,31]. Doping enough point defects into the martensitic matrix destroys the long-range ordered martensitic phase, and leads to the frozen short-range ordered strain glass state [18,19]. Furthermore, the microstructure of strain glass is a unique nanostructure with strain nanodomains dispersed into the austenite matrix [32]. Moreover, martensitic strain nanodomains are capable of growing during cooling [33] or under an external stress [34], thus leading to unique behaviors. Therefore, existence of such nanodomains is also responsible for the significant enhancement in magnetostriction by slight increase in Pd concentration in Fe-Pd FSMAs (Fig. 4).

Figures 4(a) and 4(b) exhibit the microstructure of martensite and strain glass, respectively. Figure 4(a) shows the TEM bright image of $x = 30.5$ at 90 K (below T_M), exhibiting a mesoscopic martensitic variants structure, and the corresponding electron diffraction pattern exhibits spot splitting, which is taken from the $[110]_A$ zone axis of fcc-structured austenite [35]. Comparative analysis indicates the absence of mesoscopic martensitic variants for $x = 32$ at 90 K (below T_g) [Fig. 4(b)]. Instead, nanosized martensitic domains are detected with no spot splitting in the diffraction pattern along the $[110]_A$ zone axis. From our preliminary high-resolution TEM results, the local structure of the nanodomains is likely to be tetragonal distorted. However, further work is still needed to identify the exact structural information. Oriented and short-rods-like morphology of nanodomains at $x = 32$ is observed, which is quite different from the morphology of the R-phase-like nanodomains of strain glass in Ti-Ni-based alloys [18,32]. Noteworthy, Lloveras *et al.* [36] already predicted these two morphologies of strain glass in the simulation studies on interplay between elastic anisotropy and disorder in martensites. They found the morphology of strain glass varies from "glassy droplets" to "glassy tweed" with the increase in elastic anisotropy of the system. Our work experimentally confirms their prediction on glassy tweed for the first time. These nanodomains indicate excess Pd atoms successfully suppress the formation of mesoscopic martensitic variants, and lead to a frozen nanodomains dispersive two-phase nanostructure when x ≥ 32.

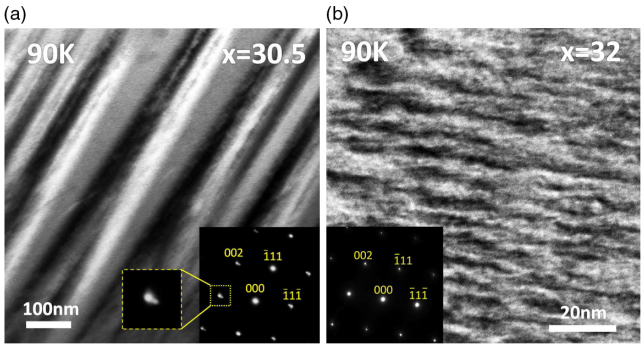

FIG. 4. (a) Long-range ordered martensitic variants for $x = 30.5$ at 90 K (below T_M) and (b) short-range ordered strain nanodomains for $x = 32$ at 90 K (below T_g).

Interestingly, a similar microstructure has also been reported in Fe-Ga alloys [37–40]. There is a two-phase nanostructure with DO_3 [ordered body-centered-cubic (bcc) phase] nanoprecipitates embedded in the $A2$ (disordered bcc phase) matrix [37,38]. Nanodomains come from the tetragonal distortion of the nanoprecipitates. Theoretical studies proposed that this type of two-phase nanostructure possesses a low structural anisotropy, indicating low energy barriers for nanodomain reorientation [39,40]. These studies well explained the "soft" nature and relative large magnetostriction of Fe-Ga alloys. However, these nanodomains in Fe-Ga alloys are also restricted by nanoprecipitates and are unable to grow under an external field owing to the chemical difference between the precipitates and the matrix. Therefore, only a limited magnetostrictive enhancement can be generated by these nanosized domains in Fe-Ga alloys due to their tiny size and low proportion in volume, although small external field is enough to induce the rotation of these nanodomains.

The microstructure of strain glass is analogous to the nanoprecipitates dispersive nanostructure of Fe-Ga alloys; therefore, strain glass can also be considered to possess low energy barriers so that strain nanodomains readily rotate at a low magnetic field. Thus, a low field can trigger a large magnetostriction in strain glass. Moreover, notably, there is a clear difference between them: the nanodomains are restricted by nanoprecipitates in Fe-Ga alloys, whereas such a restriction is absent in strain glass, owing to the chemical homogeneity of the system. Consequently, herein, the strain nanodomains are "alive" and able to grow under external stimuli such as temperature [33], stress [34], and magnetic field. Actually, the highest magnetostriction of strain glass for $x = 32.3$ is around 800 ppm in this study, significantly higher than the maximum of Fe-Ga single

crystal [5,8]. Therefore, strain glass is more promising to generate low-field-triggered large magnetostriction.

Though the concentrations of $x = 31.3$ and $x = 32.3$ are close to each other, the corresponding states are quite different. There is a long-range ordered martensitic phase with mesoscopic strain domains for $x = 31.3$; however, there is a short-range ordered strain glass state with nanosized strain domains for $x = 32.3$. Obviously, a nanodomains dispersive nanostructure is responsible for low-field-triggered large magnetostriction.

Strain glass shares a lot of similarity with ferroelectric relaxor, such as frequency dependence of responses and the broken ergodicity [18,28]. Noteworthy, similar field-induced strain behavior was also found in ferroelectric relaxors [41,42]. In ferroelectrics, a low-field-triggered large electrostriction always appears in the relaxor compositions where polar nanodomains randomly distribute in the matrix [41,42]. Thus, introducing the glass state to form nanoscale ferroic domains in the matrix may be a useful recipe to achieve a low-field-triggered large strain in ferroic materials.

Herein we reported a low-field-triggered large magnetostriction of 800 ppm by the saturation field of 0.8 kOe in Fe-Pd strain glass alloys. A magnetostriction enhancement jumping from 340 to 800 ppm by a slight deviation with 1 at. % Pd modification was observed. The microstructure of strain glass with strain nanodomains dispersed into the austenite matrix was found to be responsible for the unique magnetostrictive behavior. This study indicates that introducing nanoscale strain domains may be an effective approach to endow a number of FSMAs with novel properties, such as low-field-triggered large magnetostriction.

The authors are thankful to J. Ma, X. D. Ding, Y. Wang, D. Wang, J. Zhang, C. Zhou, and T. Y. Ma for technical support and helpful discussions. We greatly acknowledge the support from National Natural Science Foundation of China Grants (No. 51431007, No. 51471125, No. 51671157, No. 51320105014).

*senyang@mail.xjtu.edu.cn
†Ren.Xiaobing@nims.go.jp; ren.xiaobing@xjtu.edu.cn

[1] E. du Trémolet de Lacheisserie, *Magnetostriction: Theory and Applications of Magnetoelasticity* (CRC Press, Florida, 1993).
[2] F. Claeyssen, N. Lhermet, R. Le Letty, and P. Bouchilloux, J. Alloys Compd. **258**, 61 (1997).
[3] T. Honda, K. I. Arai, and M. Yamaguchi, J. Appl. Phys. **76**, 6994 (1994).
[4] E. Quandt, B. Gerlach, and K. Seemann, J. Appl. Phys. **76**, 7000 (1994).
[5] A. E. Clark, J. B. Restorff, M. Wun-Fogle, T. A. Lograsso, and D. L. Schlagel, IEEE Trans. Magn. **36**, 3238 (2000).
[6] A. E. Clark, M. Wun-Fogle, J. B. Restorff, T. A. Lograsso, and J. R. Cullen, IEEE Trans. Magn. **37**, 2678 (2001).
[7] S. Guruswamy, N. Srisukhumbowornchai, A. Clark, J. Restorff, and M. Wun-Fogle, Scr. Mater. **43**, 239 (2000).
[8] A. E. Clark, K. B. Hathaway, M. Wun-Fogle, J. B. Restorff, T. A. Lograsso, V. M. Keppens, G. Petculescu, and R. A. Taylor, J. Appl. Phys. **93**, 8621 (2003).
[9] D. Hunter, W. Osborn, K. Wang, N. Kazantseva, J. Hattrick-Simpers, R. Suchoski, R. Takahashi, M. L. Young, A. Mehta, and L. A. Bendersky, Nat. Commun. **2**, 518 (2011).
[10] A. E. Clark and H. S. Belson, Phys. Rev. B **5**, 3642 (1972).
[11] A. E. Clark, J. P. Teter, and O. D. McMasters, J. Appl. Phys. **63**, 3910 (1988).
[12] A. Sozinov, A. Likhachev, N. Lanska, and K. Ullakko, Appl. Phys. Lett. **80**, 1746 (2002).
[13] M. Chmielus, X. Zhang, C. Witherspoon, D. Dunand, and P. Müllner, Nat. Mater. **8**, 863 (2009).
[14] T. Wada, Y. Liang, H. Kato, T. Tagawa, M. Taya, and T. Mori, Mater. Sci. Eng. A **361**, 75 (2003).
[15] T. Ma, C. Jiang, and H. Xu, Appl. Phys. Lett. **86**, 162505 (2005).
[16] T. Ma, M. Yan, J. Zhang, W. Luo, C. Jiang, and H. Xu, Appl. Phys. Lett. **90**, 102502 (2007).
[17] T. Kakeshita, T. Fukuda, and T. Takeuchi, Mater. Sci. Eng. A **438–440**, 12 (2006).
[18] S. Sarkar, X. Ren, and K. Otsuka, Phys. Rev. Lett. **95**, 205702 (2005).
[19] Y. Zhou, D. Xue, X. Ding, Y. Wang, J. Zhang, Z. Zhang, D. Wang, K. Otsuka, J. Sun, and X. Ren, Acta Mater. **58**, 5433 (2010).
[20] F. Xiao, T. Fukuda, T. Kakeshita, and K. Takahashi, J. Alloys Compd. **577s**, s323 (2013).
[21] M. Matsui, H. Yamada, and K. Adachi, J. Phys. Soc. Jpn. **48**, 2161 (1980).
[22] M. Sugiyama, R. Oshima, and F. E. Fujita, Trans. JIM **25**, 585 (1984).
[23] M. Matsui and K. Adachi, Physica (Amsterdam) **161B**, 53 (1990).
[24] J. Cui, T. W. Shield, and R. D. James, Acta Mater. **52**, 35 (2004).
[25] I. Opahle, K. Koepernik, U. Nitzsche, and M. Richter, Appl. Phys. Lett. **94**, 072508 (2009).
[26] Y. Wang, Y. Zhou, J. Zhang, X. Ding, S. Yang, X. Song, X. Ren, and K. Otsuka, Acta Mater. **58**, 4723 (2010).
[27] See Supplemental Material at http://link.aps.org/supplemental/10.1103/PhysRevLett.119.125701 for Fig. 1 shows the fitting curves of Cole-Cole plots and the relaxation spectrums at several temperatures for $x = 32$. Figure 2 exhibits the XRD profiles across T_M for $x = 30.5$ and T_0 for $x = 32$ respectively. Figure 3 shows HREM images of martensitic precursor for $x = 30.5$ at room temperature.
[28] Y. Wang, X. Ren, K. Otsuka, and A. Saxena, Phys. Rev. B **76**, 132201 (2007).
[29] D. Viehland, J. F. Li, S. J. Jang, L. E. Cross, and M. Wuttig, Phys. Rev. B **46**, 8013 (1992).
[30] N. Gayathri, A. K. Raychaudhuri, S. K. Tiwary, R. Gundakaram, A. Arulraj, and C. N. R. Rao, Phys. Rev. B **56**, 1345 (1997).
[31] Y. Wang, C. Huang, J. Gao, S. Yang, X. Ding, X. Song, and X. Ren, Appl. Phys. Lett. **101**, 101913 (2012).
[32] Y. Zhou, D. Xue, Y. Tian, X. Ding, S. Guo, K. Otsuka, J. Sun, and X. Ren, Phys. Rev. Lett. **112**, 025701 (2014).
[33] J. Zhang, Y. Wang, X. Ding, Z. Zhang, Y. Zhou, X. Ren, D. Wang, Y. Ji, M. Song, K. Otsuka, and J. Sun, Phys. Rev. B **84**, 214201 (2011).

[34] Y. Wang, X. Ren, and K. Otsuka, Phys. Rev. Lett. **97**, 225703 (2006).
[35] M. Sugiyama, R. Oshima, and F. E. Fujita, Trans. JIM **27**, 719 (1986).
[36] P. Lloveras, T. Castán, M. Porta, A. Planes, and A. Saxena, Phys. Rev. B **80**, 054107 (2009).
[37] S. Bhattacharyya, J. R. Jinschek, A. Khachaturyan, H. Cao, J. F. Li, and D. Viehland, Phys. Rev. B **77**, 104107 (2008).
[38] H. Cao, P. M. Gehring, C. Devreugd, J. A. Rodriguez-Rivera, J. Li, and D. Viehland, Phys. Rev. Lett. **102**, 127201 (2009).
[39] W. F. Rao, M. Wuttig, and A. G. Khachaturyan, Phys. Rev. Lett. **106**, 105703 (2011).
[40] W. F. Rao and A. G. Khachaturyan, Acta Mater. **59**, 4494 (2011).
[41] C. Ang and Z. Yu, Adv. Mater. **18**, 103 (2006).
[42] X. Liu and X. Tan, Adv. Mater. **28**, 574 (2016).